

High-level cognition is supported by information-rich but compressible brain activity patterns

Lucy L. W. Owen^{1,2} and Jeremy R. Manning^{1,*}

¹Department of Psychological and Brain Sciences,
Dartmouth College, Hanover, NH

²Carney Institute for Brain Sciences,
Brown University, Providence, RI

*Address correspondence to jeremy.r.manning@dartmouth.edu

December 21, 2023

Abstract

Brain activity patterns are highly flexible and often complex, but also highly structured. Here we examined how fundamental properties of brain activity patterns relate to ongoing cognitive processes. To this end, we applied dimensionality reduction algorithms and pattern classifiers to functional neuroimaging data collected as participants listened to a story, temporally scrambled versions of the story, or underwent a resting state scanning session. These experimental conditions were intended to require different depths of processing and inspire different levels of cognitive engagement. We considered two primary aspects of the data. First, we treated the maximum achievable decoding accuracy across participants as an indicator of the “informativeness” of the recorded patterns. Second, we treated the number of features (components) required to achieve a threshold decoding accuracy as a proxy for the “compressibility” of the neural patterns (where fewer components indicate greater compression). Overall, we found that the peak decoding accuracy (achievable without restricting the numbers of features) was highest in the intact (unscrambled) story listening condition. However, the number of features required to achieve comparable classification accuracy was also lowest in the intact story listening condition. Taken together, our work suggests that our brain networks flexibly reconfigure according to ongoing task demands, and that the activity patterns associated with higher-order cognition and high engagement are both more informative and more compressible than the activity patterns associated with lower-order tasks and lower levels of engagement.

Keywords: information, compression, temporal decoding, dimensionality reduction, neuroimaging

Significance Statement: How our brains respond to ongoing experiences depends on what we are doing and thinking about, how engaged we are, and our past experiences, among other factors. To gain insights into how brain activity patterns reflect ongoing cognitive processes, we examined two fundamental aspects of brain activity under different cognitive circumstances: informativeness and compressibility. Informativeness refers to the extent to which brain patterns are both temporally specific and consistent across different people. Compressibility refers to the extent to how robust the informativeness of brain patterns is to dimensionality reduction. We found that brain activity patterns evoked by higher-level cognitive tasks are both more informative *and* more compressible than activity evoked by lower-level tasks. Our findings suggest that our brains flexibly reconfigure themselves to optimize different aspects of how they function according to ongoing cognitive demands.

37 Introduction

38 Large-scale networks, including the human brain, may be conceptualized as occupying one or
39 more positions along on a continuum. At one extreme, every node is fully independent from
40 every other node. At the other extreme, all nodes behave identically. Each extreme optimizes
41 key properties of how the network functions. When every node is independent, the network is
42 maximally *expressive*: if we define the network's "state" as the activity pattern across its nodes, then
43 every state is equally reachable by a network with fully independent nodes. On the other hand, a
44 network of identically behaved nodes optimizes *robustness*: any subset of nodes may be removed
45 from the network without any loss of function or expressive power, as long as any single node
46 remains. Presumably, most natural systems tend to occupy positions between these extremes. We
47 wondered: might the human brain reconfigure itself to be more flexible or more robust according
48 to ongoing demands? In other words, might the brain reconfigure its connections or behaviors
49 under different circumstances to change its position along this continuum?

50 Closely related to the above notions of expressiveness versus robustness are measures of
51 how much *information* is contained in a given signal or pattern, and how *redundant* a signal
52 is (Shannon, 1948). Formally, information is defined as the amount of uncertainty about a given
53 variables' outcomes (i.e., entropy), measured in *bits*, or the optimal number of yes/no questions
54 needed to reduce uncertainty about the variable's outcomes to zero. Highly complex systems with
55 many degrees of freedom (i.e., high flexibility and expressiveness), are more information-rich than
56 simpler or more constrained systems. The redundancy of a signal denotes the difference between
57 how expressive the signal *could* be (i.e., proportional to the number of unique states or symbols
58 used to transmit the signal) and the actual information rate (i.e., the entropy of each individual
59 state or symbol). If a brain network's nodes are fully independent, then the number of bits required
60 to express a single activity pattern is proportional to the number of nodes. The network would
61 also be minimally redundant, since the status of every node would be needed to fully express a
62 single brain activity pattern. If a brain network's nodes are fully coupled and identical, then the
63 number of bits required to express a single activity pattern is proportional to the number of unique
64 states or values any individual node can take on. Such a network would be highly redundant,
65 since knowing any individual node's state would be sufficient to recover the full-brain activity

66 pattern. Highly redundant systems are also robust, since there is little total information loss due
67 to removing any given observation.

68 We take as a given that brain activity is highly flexible: our brains can exhibit nearly infinite
69 varieties of activity patterns. This flexibility implies that our brains' activity patterns are highly
70 information rich. However, brain activity patterns are also highly structured. For example,
71 full-brain correlation matrices are stable within (Finn et al., 2017, 2015; Gratton et al., 2018) and
72 across (Cole et al., 2014; Glerean et al., 2012; Gratton et al., 2018; Yeo et al., 2011) individuals. This
73 stability suggests that our brains' activity patterns are at least partially constrained, for example
74 by anatomical, external, or internal factors. Constraints on brain activity that limit its flexibility
75 decrease expressiveness (i.e., its information rate). However, constraints on brain activity also
76 increase its robustness to noise (e.g., "missing" or corrupted signals may be partially recovered).
77 For example, recent work has shown that full-brain activity patterns may be reliably recovered
78 from only a relatively small number of implanted electrodes (Owen et al., 2020; Scangos et al.,
79 2021). This robustness property suggests that the relevant signal (e.g., underlying factors that
80 have some influence over brain activity patterns) are compressible.

81 To the extent that brain activity patterns contain rich task-relevant information, we should be
82 able to use the activity patterns to accurately differentiate between different aspects of a task (e.g.,
83 using pattern classifiers; Norman et al., 2006). For example, prior work has shown a direct
84 correspondence between classification accuracy and the information content of a signal (Alvarez,
85 2002). To the extent that brain activity patterns are compressible, we should be able to generate
86 simplified (e.g., lower dimensional) representations of the data while still preserving the relevant
87 or important aspects of the original signal. In general, information content and compressibility
88 are often related but are also dissociable (Fig. 1). If a given signal (e.g., a representation of brain
89 activity patterns) contains more information about ongoing cognitive processes, then the peak
90 decoding accuracy should be high. In the simulations shown in Figure 1C we construct synthetic
91 datasets that have high or low levels of informativeness by varying temporal autocorrelations
92 in the data (see *Synthetic data*). If a signal is compressible, then a low-dimensional embedding
93 of the signal will be similarly informative as the original signal. In the simulations shown in
94 Figure 1C we construct synthetic datasets that have high or low levels of compressibility by
95 varying the covariance structure across features (see *Synthetic data*). As shown in Figure 1D, highly

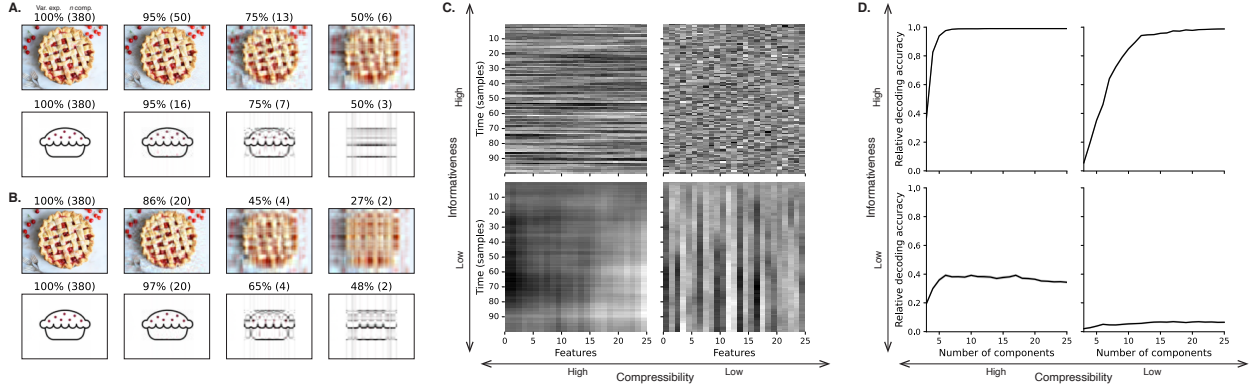


Figure 1: Information content and compressibility. **A. Variance explained for two images.** Consider two example images: a photograph and simple drawing. The images have the same resolutions, but their content is very different. The photograph is more information rich: when we compare the original photograph and drawing (leftmost column), we can see that the photograph captures much more detail. We can also apply principal components analysis to the images, treating the rows of the images as “observations.” Across columns, we identified the numbers of components required to explain 100%, 95%, 75%, or 50% of the cumulative variance in each image (the 100% columns denote the original images). The numbers of components are indicated in parentheses, and the resulting “compressed” images are displayed. This analysis reveals that the drawing is more compressible: just 16 components can explain 95% of the variance in the drawing, whereas 50 components are required to explain 95% of the variance in the photograph. **B. Representing two images with different numbers of components.** Using the same principal component decompositions as in Panel A, we computed the cumulative proportion of variance explained with 380 (original images), 20, 4, or 2 components. This analysis provides another way of characterizing the compressibility of each image by showing that the same number of components can explain more variance in the drawing than in the photograph. **C. Template data from four synthetic datasets.** We constructed four synthetic datasets, each comprising 25 features (columns) observed across 100 samples (rows) from each of 10 simulated “participants.” The datasets were constructed to contain different levels of informativeness and compressibility (see *Synthetic data*). **D. Decoding accuracy by number of components.** For each synthetic dataset, we trained across-participant classifiers to decode timepoint labels. Each panel displays the decoding accuracy as a function of the number of components used to represent the data. Error ribbons denote bootstrap-estimated 95% confidence intervals.

96 informative datasets yield higher decoding accuracies than less informative datasets (i.e., the peaks
97 of the curves in the top panels of Fig. 1D are higher than the peaks of the curves in the bottom
98 panels). Highly compressible datasets show steeper slopes when we plot decoding accuracy as a
99 function of the number of components used to represent the data (i.e., the slopes of the curves in
100 the left panels of Fig. 1D are steeper than the slopes of the curves in the right panels). Whereas
101 characterizing the informativeness and compressibility of synthetic data can be instructive, we
102 are ultimately interested in understanding how these properties relate to brain activity patterns
103 recorded under different cognitive circumstances.

104 Several recent studies suggest that the complexity of brain activity is task-dependent, whereby
105 simpler tasks with lower cognitive demands are reflected by simpler and more compressible brain
106 activity patterns, and more complex tasks with higher cognitive demands are reflected by more
107 complex and less compressible brain activity patterns (Mack et al., 2020; Owen et al., 2021). These
108 findings complement other work suggesting that functional connectivity (correlation) patterns are
109 task-dependent (Cole et al., 2014; Finn et al., 2017; Owen et al., 2020), although see Gratton et
110 al. (2018). Higher-order cognitive processing of a common stimulus also appears to drive more
111 stereotyped task-related activity and functional connectivity across individuals (Hasson et al.,
112 2008; Lerner et al., 2011; Simony & Chang, 2020; Simony et al., 2016).

113 The above studies are consistent with two potential descriptions of how cognitive processes are
114 reflected in brain activity patterns. One possibility is that the information rate of brain activity in-
115 creases during more complex or higher-level cognitive processing. If so, then the ability to reliably
116 decode cognitive states from brain activity patterns should improve with task complexity or with
117 the level (or “depth”) of cognitive processing. A second possibility is that the compressibility of
118 brain activity patterns increases during more complex or higher-level cognitive processing. If so,
119 then individual features of brain recordings, or compressed representations of brain recordings,
120 should carry more information during complex or high-level (versus simple or low-level) cognitive
121 tasks.

122 We used a previously collected neuroimaging dataset to estimate the extent to which each of
123 these two possibilities might hold. The dataset we examined comprised functional magnetic reso-
124 nance imaging (fMRI) data collected as participants listened to an audio recording of a 10-minute
125 story, temporally scrambled recordings of the story, or underwent a resting state scan (Simony

126 et al., 2016). Each of these experimental conditions evokes different depths of cognitive process-
127 ing (Hasson et al., 2008; Lerner et al., 2011; Owen et al., 2021; Simony et al., 2016). We used
128 across-participant classifiers to decode listening times in each condition, as a proxy for how “infor-
129 mative” the task-specific activity patterns were (Simony & Chang, 2020). We also used principle
130 components analysis to generate lower-dimensional representations of the activity patterns. We
131 then repeated the classification analyses after preserving different numbers of components and
132 examined how classification accuracy changed across the different experimental conditions.

133 Results

134 We sought to understand whether higher-level cognition is reflected by more reliable and in-
135 formative brain activity patterns, and how compressibility of brain activity patterns relates to
136 cognitive complexity. We developed a computational framework for systematically assessing the
137 informativeness and compressibility of brain activity patterns recorded under different cognitive
138 circumstances. We used across-participant decoding accuracy (see *Forward inference and decoding*
139 *accuracy*) as a proxy for informativeness. To estimate the compressibility of the brain patterns, we
140 used group principal components analysis (PCA) to project the brain patterns into k -dimensional
141 spaces, for different values of k (see *Hierarchical Topographic Factor Analysis (HTFA)* and *Principal*
142 *components analysis (PCA)*). For more compressible brain patterns, decoding accuracy should be
143 more robust to small values of k .

144 We analyzed a dataset collected by Simony et al. (2016) that comprised four experimental con-
145 ditions. These conditions exposed participants to stimuli that systematically varied in cognitive
146 engagement. In the *intact* experimental condition, participants listened to an audio recording of a
147 10-minute Moth Radio Hour story, *Pie Man*, by Jim O’Grady. In the *paragraph*-scrambled experi-
148 mental condition, participants listened to a temporally scrambled version of the story, where the
149 paragraphs occurred out of order, but where the same set of paragraphs was presented over the
150 entire listening interval. All participants in this condition experienced the scrambled paragraphs
151 in the same order. In the *word*-scrambled experimental condition, participants listened to a tem-
152 porally scrambled version of the story, where the words occurred in a random order. Again, all
153 participants in this condition experienced the scrambled words in the same order. Finally, in the

154 *rest* experimental condition, participants lay in the scanner with no overt stimulus, while keeping
155 their eyes open and blinking as needed. This public dataset provided a convenient means for
156 testing our hypothesis that different levels of cognitive processing and engagement affect how
157 informative and compressible the associated brain patterns are.

158 To evaluate the relation between informativeness and compressibility for brain activity from
159 each experimental condition, we trained a series of across-participant temporal decoders on com-
160 pressed representations of the data. Figure 2A displays the decoding accuracy as a function
161 of the number of principal components used to represent the data (also see Fig. S1). Several
162 patterns were revealed by the analysis. First, in general (i.e., across experimental conditions),
163 decoding accuracy tends to improve as the number of components are increased. However, de-
164 coding accuracy peaked at higher levels for experimental conditions that exposed participants
165 to cognitively richer stimuli (Fig. 2D). The peak decoding accuracy was highest for the “intact”
166 condition (versus paragraph: $t(99) = 35.205, p < 0.001$; versus word: $t(99) = 43.172, p < 0.001$);
167 versus rest: $t(99) = 81.361, p < 0.001$), next highest for the “paragraph” condition (versus word:
168 $t(99) = 6.243, p < 0.001$; versus rest: $t(99) = 50.748, p < 0.001$), and next highest for the “word”
169 condition (versus rest: $t(99) = 48.791, p < 0.001$). This ordering implies that cognitively richer
170 conditions evoke more stable brain activity patterns across people.

171 The cognitively richer conditions also displayed steeper initial slopes. For example, the intact
172 condition decoders reached an arbitrarily chosen threshold of 5% accuracy using fewer components
173 than the paragraph condition decoders ($t(99) = -7.429, p < 0.001$) or word condition decoders
174 ($t(99) = -7.300, p < 0.001$), and decoding accuracy never exceeded 5% for the rest condition. This
175 suggests that brain activity patterns evoked by cognitively richer conditions are more compressible,
176 such that representing the data using the same number of principal components provides more
177 information to the temporal decoders (Figs. 2B, C). Taken together, as shown in Figure 2E, we
178 found that brain activity patterns evoked by cognitively richer conditions tended to be both more
179 informative (i.e., associated with higher peak decoding accuracies) *and* more compressible (i.e.,
180 requiring fewer components to achieve the 5% accuracy threshold).

181 If informativeness (to the temporal decoders) and compressibility vary with the cognitive
182 richness of the stimulus, might these measures also vary over time *within* a given condition? For
183 example, participants in the intact condition might process the ongoing story more deeply later

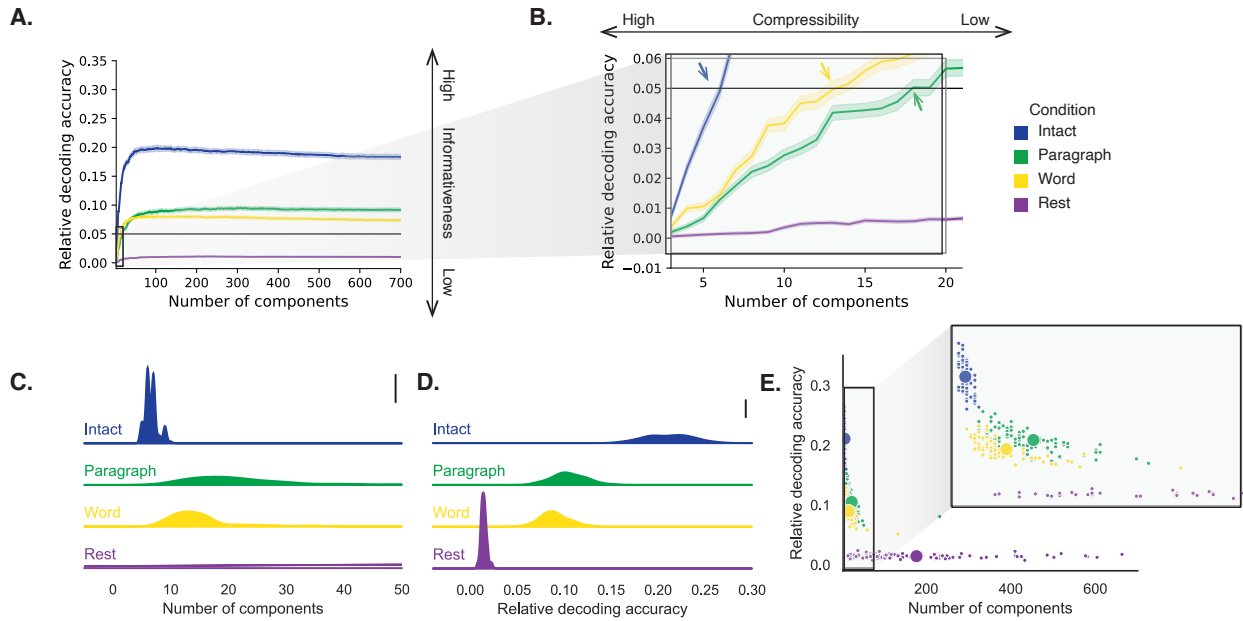


Figure 2: Decoding accuracy and compressibility.

A. Decoding accuracy by number of components. Ribbons of each color display cross-validated decoding performance for each condition (intact, paragraph, word, and rest), as a function of the number of components (features) used to represent the data. For each condition, decoding accuracy has been normalized by subtracting expected “chance” decoding performance (estimated as $\frac{1}{T}$, where T is the number of timepoints in the given condition). This normalization was intended to enable fairer comparisons across conditions; a relative decoding accuracy of 0.0 denotes “chance” performance. The horizontal black line denotes 5% decoding accuracy (used as a reference in Panel B).

B. Numbers of components required to reach a fixed decoding accuracy threshold, by condition. The panel displays a zoomed-in view of the inset in Panel A. Intersections between each condition’s decoding accuracy curve and the 5% decoding accuracy reference line are marked by arrows. All error ribbons in Panels A and B denote bootstrap-estimated 95% confidence intervals.

C. Estimating “compressibility” for each condition. The probability density plots display the numbers of components required to reach at least 5% (corrected) decoding accuracy, across all cross validation runs. For the “rest” condition, where decoding accuracy never reached 5% accuracy, we display the distribution of the numbers of components required to achieve the peak decoding accuracy in each fold. (This distribution is nearly flat, as also illustrated in Panel E.) The scale bar denotes a height of 0.01.

D. Estimating “informativeness” for each condition. The probability density plots display the peak (corrected) decoding accuracies achieved in each condition, across all cross validation runs. The scale bar denotes a height of 0.01.

E. Informativeness versus compressibility. Each dot displays the minimum number of components required to achieve at least 5% corrected decoding accuracy (x -coordinate; for the rest condition the numbers of components are estimated using the peak decoding accuracies as in Panel C) and the peak (corrected) decoding accuracy (y -coordinate). The smaller dots correspond to individual cross validation runs and the larger dots display the averages across runs. The inset displays a zoomed-in view of the indicated region in the main panel.

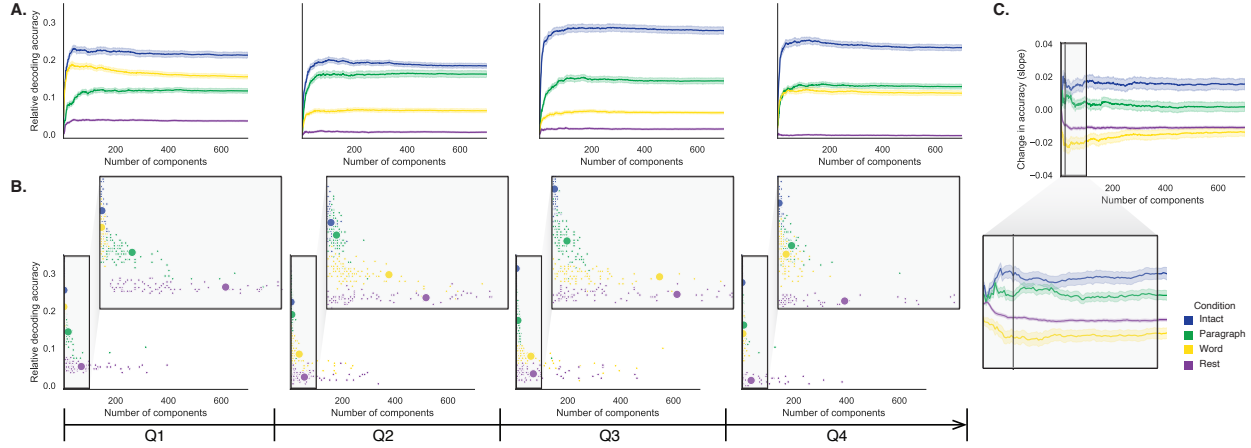


Figure 3: Changes in decoding accuracy and compression over time. **A. Decoding accuracy by number of components, by story segment.** Each family of curves is plotted in the same format as Figure 2A but reflects data only from one quarter of the dataset. **B. Informativeness versus compressibility by condition and segment.** Each scatter plot is in the same format as Figure 2E, but reflects data only from one quarter of the dataset. **C. Change in decoding accuracy over time, by number of components.** For each number of components (x -axis) and condition (color), we fit a regression line to the decoding accuracies obtained for the first, second, third, and fourth quarters of the dataset (corresponding to the columns of Panels A and B). The y -axis denotes the slopes of the regression lines. The black vertical line marks $k = 20$ components, as referenced in the main text. All error ribbons denote bootstrap-estimated 95% confidence intervals.

on in the story (compared with earlier in the story) given the additional narrative background and context they had been exposed to by that point. To examine this possibility, we divided each condition into four successive time segments. We computed decoding curves (Fig. 3A) and the numbers of components required to achieve 5% decoding accuracy (Fig. 3B) for each segment and condition. We found that, in the two most cognitively rich conditions (intact and paragraph), both decoding accuracy and compressibility, as reflected by the change in decoding curves, increased with listening time (e.g., at the annotated reference point of $k = 20$ components in Fig. 3C: intact: $t(99) = 7.915, p < 0.001$; paragraph: $t(99) = 2.354, p = 0.021$). These changes may reflect an increase in comprehension or depth of processing with listening time. In contrast, the decoding accuracy and compressibility decreased with listening time in the word condition ($t(99) = -10.747, p < 0.001$) and rest condition ($t(99) = -22.081, p < 0.001$). This might reflect the depletion of attentional resources in the less-engaging word and rest conditions.

These results make some intuitive sense. As the contextual information available to participants increases (i.e., over time in the cognitively rich intact and paragraph conditions), it makes sense that

198 this might constrain neural responses to a greater extent. While this pattern may not necessarily
199 hold for *every* possible story or stimulus, we suspect that it is generally the case that our knowledge
200 about what is happening in a story tends to increase as we experience more about it. In turn, this
201 could lead to greater consistency in different people's interpretations of and neural responses to
202 the stimulus. Similarly, as participants are left to "mind wander," or as they experience mental
203 fatigue (i.e., over time in the less cognitively rich word and rest conditions), we suggest that this
204 might lead to greater variability in neural responses across people, resulting in lower decoding
205 accuracy. Again, it is not necessarily the case that every possible "unengaging" stimulus will
206 lead to greater neural variability as time progresses, but we suspect this phenomenon is likely to
207 hold for a variety of such stimuli. These findings replicate at least to a limited extent (e.g., across
208 both cognitively rich conditions and across both cognitively impoverished conditions, and for the
209 different groups of participants in each of those conditions). However, determining whether these
210 patterns generalize to other stimuli would require additional study (with new stimuli).

211 If the informativeness and compressibility of brain activity patterns vary over time, do these
212 properties might also vary across brain networks? We used a network parcellation identified by Yeo
213 et al. (2011) to segment the brain into seven distinct networks. The networks can be sorted (roughly)
214 in order from lower-level to higher-level cortex as follows (Figs. 4A–C): visual, somatomotor,
215 dorsal attention, ventral attention, limbic, frontoparietal, and default mode. Next, we computed
216 decoding curves separately for the activity patterns within each network and identified each
217 network's inflection point, for each experimental condition. Moving from low-order networks
218 to higher-order networks, we found that decoding accuracy tended to increase in the higher-
219 level experimental conditions and decrease (slightly) in the lower-level experimental conditions
220 (Fig. 4D, E; Spearman's rank correlation between decoding accuracy and network order: intact:
221 $\rho = 0.362, p < 0.001$; paragraph: $\rho = 0.441, p < 0.001$; word: $\rho = -0.102, p = 0.007$; rest: $\rho =$
222 $-0.354, p < 0.001$). This suggests that higher-order networks may carry more content-relevant
223 or stimulus-driven "information." We found no clear trends in the proportions of components
224 required to achieve 5% decoding accuracy across networks or conditions (Fig. 4F).

225 Whereas the above analyses examine different networks in isolation, how does full-brain
226 (i.e., potentially multi-network) activity patterns reflected by different principal components vary
227 across different experimental conditions? As shown in Figure 5, we used Neurosynth (Rubin et al.,

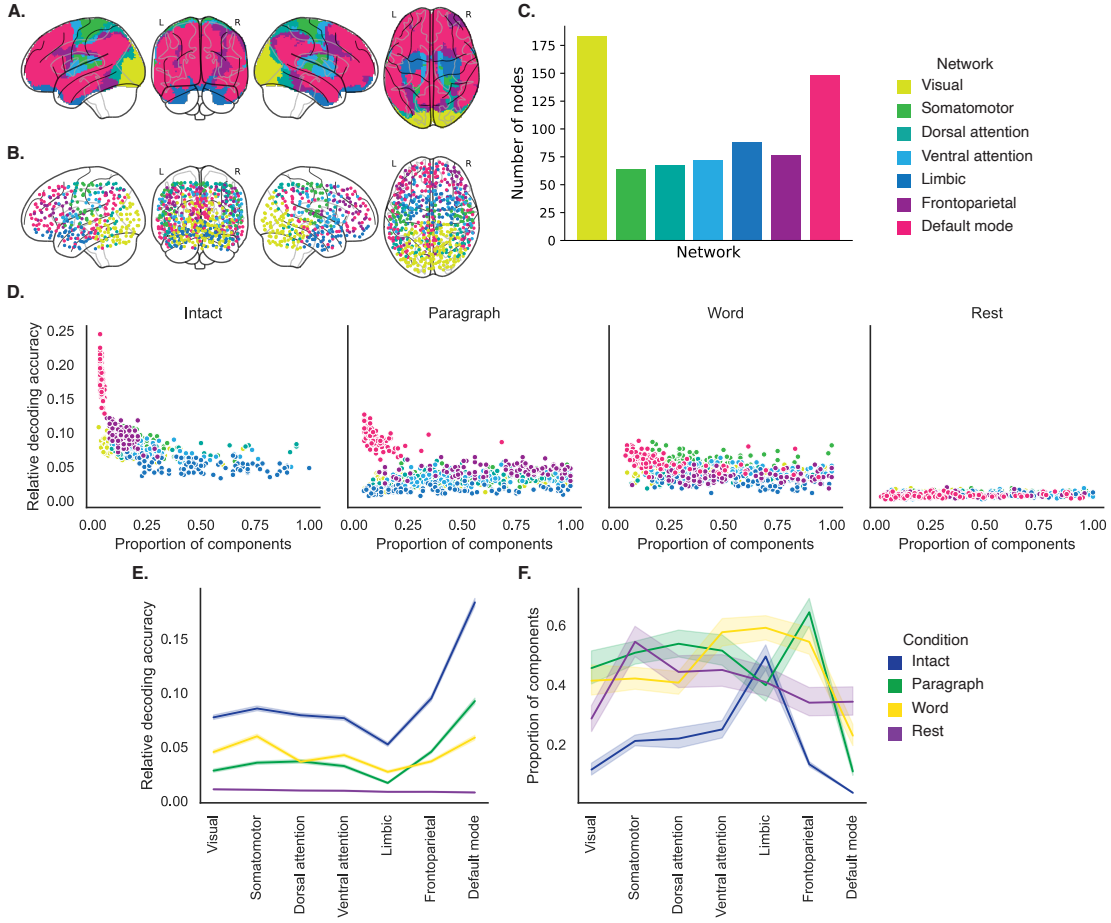


Figure 4: Network-specific decoding accuracy and compression. **A. Network parcellation map.** The glass brain displays the location of each of seven networks identified by Yeo et al. (2011). **B. Node labels.** We assigned network labels to each of 700 Hierarchical Topographic Factor Analysis-derived nodes (see *Hierarchical topographic factor analysis (HTFA)*). For each node, we evaluated its radial basis function (RBF) at the locations of every voxel in the parcellation map displayed in Panel A. We summed up these RBF weights separately for the voxels in each network. We defined each node's network label as its highest-weighted network across all voxels. **C. Per-network node counts.** The bar plot displays the total number of HTFA-derived nodes assigned to each network. **D. Informativeness versus compressibility by network and condition.** Each dot corresponds to a single cross validation run. The dots' coordinates denote the minimum proportion of components (relative to the number of nodes in the given network) required to achieve at least 5% corrected decoding accuracy (x -coordinate; for the rest condition these proportions are estimated using the peak decoding accuracies) and peak (corrected) decoding accuracy (y -coordinate). We repeated the analysis separately for each network (color) and experimental condition (column). **E. Informativeness by network.** For each network, sorted (roughly) from lower-order networks on the left to higher-order networks on the right, the curves display the peak (corrected) decoding accuracy for each experimental condition (color). **F. Compressibility by network.** For each network, the curves display the proportion of components (relative to the total possible number of components displayed in Panel C) required to achieve at least 5% decoding accuracy (or, for the rest condition, peak decoding accuracy, as described above). Error ribbons in Panels E and F denote bootstrap-estimated 95% confidence intervals.

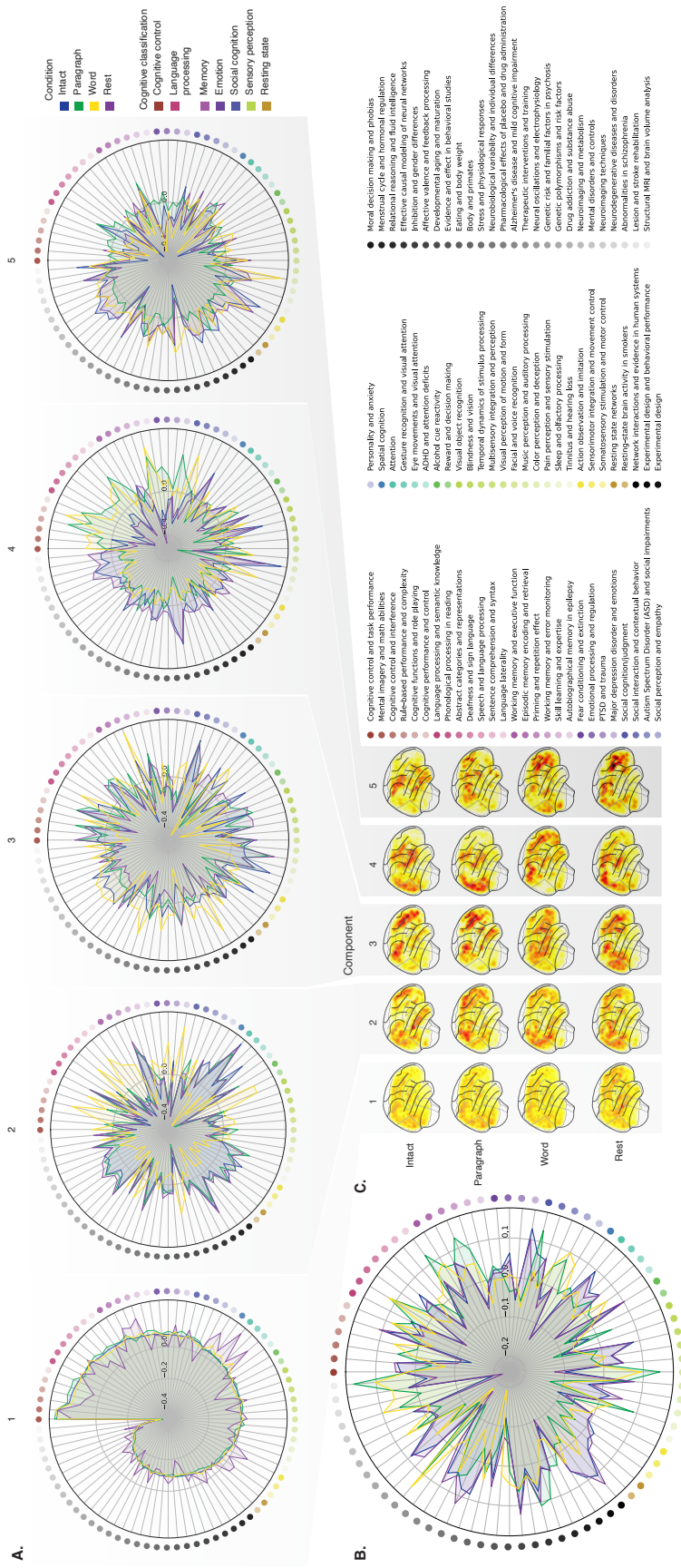


Figure 5: Neurosynth topic weightings by component. We used a reverse inference procedure (see *Reverse inference*) to estimate the correspondences between brain images and a set of 80 topics derived from the Neurosynth database of neuroimaging articles (Rubin et al., 2017). **A. Topic correlations by component.** For each of the top five highest-weighted principal components (columns) derived from each experimental condition (colors), the radar plots display the correlations between the component images and the per-topic images derived for each topic (topic identities are denoted by the blue dots; a legend for the topic labels is in the lower right of the figure). An annotated list of the top-weighted topics for each component and condition may be found in Figure S2 and the top-weighted terms for each topic may be found in Table S1. **B. Topic correlations averaged across components.** The radar plot is in the same format as the plots in Panel A, but here we display the per-condition average correlations across the top five components (for each condition) reflected in Panel A. **C. Component images.** Each plot displays a right sagittal view of a glass brain projection of the top five principal components (columns) for each experimental condition (rows). Additional projections for each component may be found in Figure S3.

²²⁸ 2017) to identify, for each component, the associations with each of 80 themes (see *Reverse inference*).
²²⁹ In general, the first principal components across all of the experimental conditions tended to weight
²³⁰ most heavily on themes related to cognitive control, memory, language processing, attention, and
²³¹ perception. Other components appeared to vary more across conditions.

²³² To gain further insights into which brain functions might be most closely associated with
²³³ the top-weighted components from each experimental condition, we manually grouped each
²³⁴ Neurosynth-derived topic into a smaller set of core cognitive functions. Separately for each com-
²³⁵ ponent, we computed the average weightings across all topics that were tagged as being associated
²³⁶ with each of these cognitive functions (Figs. 6A, S5A). To help visualize these associations, we used
²³⁷ the patterns of associations for each component to construct graphs whose nodes were experimen-
²³⁸ tal conditions and cognitive functions (Figs. 6B, S5B). We also computed correlations between the
²³⁹ sets of per-topic weightings from each of the top-weighted components from each experimental
²⁴⁰ condition (Fig. 6C, D) and between the brain maps for each condition's components (Fig. S5C, D).
²⁴¹ Taken together, we found that each component appeared to weight on a fundamental set of cogni-
²⁴² tive functions that varied by experimental condition. For example, the top principal components
²⁴³ from every condition weighted similarly (across conditions) on the full set of Neurosynth topics
²⁴⁴ (Fig. 5A) and cognitive functions (Figs. 6A, B and S5 A, B), suggesting that these components might
²⁴⁵ reflect a set of functions or activity patterns that are common across all conditions. The second
²⁴⁶ components' weightings were similar across the intact, paragraph, and rest conditions (highest-
²⁴⁷ weighted functions: cognitive control, memory, social cognition, and resting state), but different
²⁴⁸ for the word condition (highest-weighted functions: sensory perception and cognitive control).
²⁴⁹ The fourth components' weighting grouped the paragraph and word conditions (highest-weighted
²⁵⁰ functions: memory, language processing, and cognitive control) and the intact and rest conditions
²⁵¹ (highest-weighted functions: emotion, social cognition). We also used ChatGPT (OpenAI, 2023)
²⁵² to sort the list of manually tagged cognitive functions from lowest-level to highest-level (Tab. S2,
²⁵³ Fig. 6E; also see *Ranking cognitive processes*). We found that higher-level functions tended to be
²⁵⁴ weighted on more heavily by top components from the intact and paragraph conditions than lower-
²⁵⁵ level functions (intact vs. word: $t(198) = 11.059, p < 0.001$; intact vs. rest: $t(198) = 3.699, p < 0.001$;
²⁵⁶ paragraph vs. word: $t(198) = 13.504, p < 0.001$; paragraph vs. rest: $t(198) = 4.812, p < 0.001$; also
²⁵⁷ see *Ranking cognitive processes*). The top components from the word condition showed the opposite

258 tendency, whereby *lower*-level functions tended to be weighted on more heavily than higher-level
259 functions (word vs. rest: $t(198) = -7.315, p < 0.001$). The weighting trends for the intact and
260 paragraph conditions were not reliably different ($t(198) = -0.479, p = 0.633$). The components
261 from the rest condition showed almost no differences in the weights associated with high-level
262 versus low-level functions (rest vs. 0: $t(99) = 1.836, p = 0.081$). These findings suggest that when
263 participants were engaged more strongly (in the more engaging intact and paragraph conditions),
264 their dominant neural patterns reflected higher-level cognitive functions. In contrast, when partic-
265 ipants were engaged less strongly (in the less engaging word and rest conditions), their dominant
266 neural patterns reflected lower-level cognitive functions. Although they were highly statistically
267 reliable, it is also important to note that these latter effects are also relatively small (e.g., the slopes
268 for *all* of the experimental conditions are numerically close to zero; Fig. 6E). We suggest that this
269 phenomenon may merit further investigation in future work.

270 Discussion

271 We examined fMRI data collected as participants listened to an auditory recording of a story, scram-
272 bled recordings of the story, or underwent a resting state scan. We found that cognitively richer
273 stimuli evoked more reliable (i.e., consistent across people) and information rich brain activity pat-
274 terns. The brain patterns evoked by cognitively richer stimuli were also more compressible, in that
275 each individual component provided more “signal” to temporal decoders relative to components
276 of data from less cognitively rich conditions (Fig. 2). Over time (e.g., as the experiment progressed),
277 these phenomena were strengthened. Specifically, across story segments, data from more cogni-
278 tively rich conditions became more informative and compressible, and data from less cognitively
279 rich conditions became *less* informative and compressible (Fig. 3). We also repeated these analyses
280 separately for different brain networks. We found that networks traditionally associated with
281 higher-level cognitive functions tended to provide more informative brain patterns than networks
282 traditionally associated with lower level cognitive functions (Fig. 4). Finally, we examined the most
283 dominant components of the brain activity patterns from each experimental condition. We used a
284 reverse inference approach (Rubin et al., 2017) to identify the terms in the neuroimaging literature
285 most commonly associated with the corresponding maps. As summarized in Figure 6E, we found

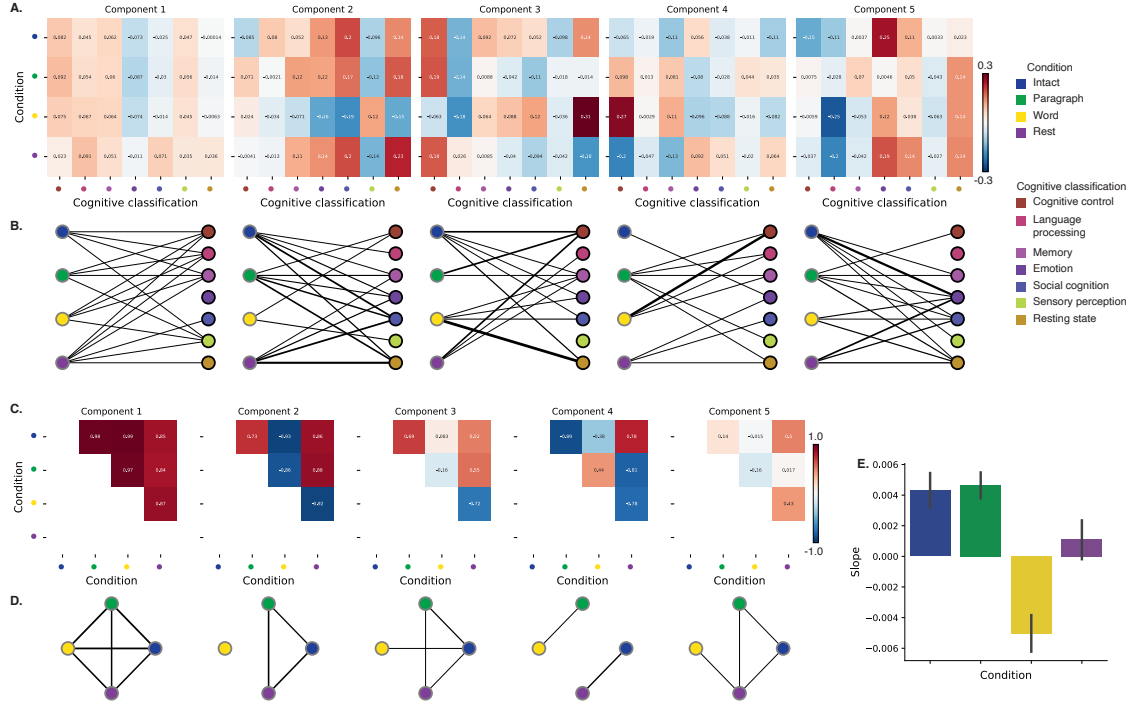


Figure 6: Summary of functions associated with top-weighted components by condition. A. Top-weighted topics by condition. Here we display per-condition (rows, indicated by colored dots) topic correlations, averaged across topics that pertain to each of several broad cognitive functions (columns within each sub-panel, indicated by colored dots). Each sub-panel reflects correlations for the components indicated in the panel titles. A legend for the condition and several core cognitive function classifications is displayed in the lower right of the figure. Table S1 provides a list of each topic's top-weighted terms, along with each topic's manually labeled cognitive classification. A full list of the topics most highly associated with each component may be found in Figure S2. **B. Associations between per-condition components and cognitive functions.** The network plots denote positive average correlations between the component images for each condition (gray-outlined dots on the left sides of each network; colors denote conditions) and topic-specific brain maps associated with each indicated cognitive function (black-outlined dots on the right sides of each network; colors denote cognitive functions). The line thicknesses are proportional to the correlation values (correlation coefficients are noted in the heat maps in Panel A). **C. Correlations between each principal component, by condition.** The heat maps display the correlations between the brain maps (Fig. S3) for each principal component (sub-panel), across each pair of conditions (rows and columns of each sub-panel's matrix, indicated by colored dots). **D. Associations between per-condition components, by component.** Each sub-panel's network plot summarizes the pattern of correlations between the n^{th} top-weighted principal components (sub-panel) for each experimental condition (gray-outlined dots). The line thicknesses are proportional to the correlation values (correlation coefficients are noted in the heat maps in Panel C). **E. Change in weights by condition.** The bar heights reflect the slopes of regression lines, fit separately to the top five components from each condition, between the ChatGPT-derived “rank” of each cognitive classification and the correlations between the component and topic maps associated with cognitive processes at the given rank (see *Ranking cognitive processes*) Error bars denote bootstrap-estimated 95% confidence intervals. Also see Fig. S5 for additional information.

286 that the intact and paragraph conditions tended to weight on higher-level cognitive processes
287 more than lower-level cognitive processes, whereas the word condition weighted on lower-level
288 processes more than higher-level processes and the rest condition showed no difference in high-
289 level versus low-level weighting. Taken together, our findings indicate that the informativeness
290 and compressibility of our brain activity patterns are task-dependent, and these properties change
291 systematically with factors like cognitive richness and depth of processing.

292 Our explorations of informativeness and compressibility are related to a much broader litera-
293 ture on the correlational and causal structure of brain activity patterns and networks (Adachi et
294 al., 2012; Bassett & Sporns, 2017; Brovelli et al., 2004; Bullmore & Sporns, 2009; Dhamala et al.,
295 2008; Korzeniewska et al., 2008; Lynn & Bassett, 2021; Owen et al., 2021; Preti et al., 2017; Rogers
296 et al., 2007; Rubinov & Sporns, 2010; Sizemore et al., 2018; Smith, Beckmann, et al., 2013; Smith,
297 Vidaurre, et al., 2013; Sporns & Betzel, 2016; Sporns & Honey, 2006; Sporns & Zwi, 2004; Srinivasan
298 et al., 2007; Tomasi & Volkow, 2011; Yeo et al., 2011). Correlations or causal associations between
299 different brain regions simultaneously imply that full-brain activity patterns will be compressible
300 and also that those activity patterns will contain redundancies. For example, the extent to which
301 activity patterns at one brain area can be inferred or predicted from activity patterns at other
302 areas (e.g., Owen et al., 2020; Scangos et al., 2021), reflects overlap in the information available
303 in or represented by those brain areas. If brain patterns in one area are recoverable using brain
304 patterns in another area, then a “signal” used to convey the activity patterns could be compressed
305 by removing the recoverable activity. Predictable (and therefore redundant) brain activity patterns
306 are also more robust to signal corruption. For example, even if the activity patterns at one region
307 are unreadable or unreliable at a given moment, that unreliability could be compensated for by
308 other regions’ activity patterns that were predictive of the unreliable region.

309 Our findings that informativeness and compressibility change with task demands may follow
310 from task-dependent changes in full-brain correlation patterns. A number of prior studies have
311 found that so-called “functional connectivity” (i.e., correlational) patterns vary reliably across
312 tasks, events, and situations (Cole et al., 2014; Owen et al., 2021; Simony et al., 2016; Smith et
313 al., 2009). By examining how these task-dependent changes in correlations affect informativeness
314 and compressibility, our work suggests a potential reason why the statistical structure of brain
315 activity patterns might vary with cognitive task or with cognitive demands. For lower-level tasks,

316 or for tasks that require relatively little “deep” cognitive processing, our brains may optimize
317 activity patterns for robustness and redundancy over expressiveness, for example to maximize
318 reliability. For higher-level tasks, or for tasks that require deeper cognitive processing, our brains
319 may sacrifice some redundancy in favor of greater expressiveness.

320 In the information theory sense (Shannon, 1948), when a signal is transmitted using a fixed
321 alphabet of “symbols,” the information rate decreases as the signal is compressed (e.g., fewer sym-
322 bols transmitted per unit time, using an alphabet with fewer symbols, etc.). Our finding that each
323 individual brain component (symbol) becomes more informative as cognitive richness increases
324 suggests that the “alphabet” of brain activity patterns is also task-dependent. Other work suggests
325 that the representations that are *reflected* by brain activity patterns may also change with task de-
326 mands. For example, our brains may represent the same perceptual stimulus differently depending
327 on which aspects of the stimulus or which combinations of features are task-relevant (Mack et al.,
328 2020).

329 Different brain networks also varied in how informative and compressible their activity pat-
330 terns were across experimental conditions (e.g., Fig. 4). This might follow from evolutionary
331 optimizations that reflect the relevant constraints or demands placed on those networks. One
332 possibility is that cortex is organized in a hierarchy of networks “concerned with” or selective to
333 different levels of processing or function. To the extent that different levels of processing (e.g.,
334 low-level sensory processing versus “deeper” higher-level processing) reflect different stimulus
335 timescales (e.g., Manning, 2020), the network differences we observed might also relate to the
336 timescales at which each network is maximally sensitive (Baldassano et al., 2017; Hasson et al.,
337 2008; Lerner et al., 2011; Regev et al., 2018).

338 **Concluding remarks**

339 Cognitive neuroscientists are still grappling with basic questions about the fundamental “rules”
340 describing how our brains respond, and about how brain activity patterns and the associated
341 underlying cognitive representations and computations are linked. We identified two aspects of
342 brain activity patterns, informativeness and compressibility, that appear to change systematically
343 with task demands and across brain networks. Our work helps to clarify how the “neural code”

³⁴⁴ might be structured, and how the code might vary across tasks and brain areas.

³⁴⁵ Methods

³⁴⁶ We measured properties of recorded neuroimaging data under different task conditions that varied
³⁴⁷ systematically in cognitive engagement and depth of processing. We were especially interested in
³⁴⁸ how *informative* and *compressible* the activity patterns were under these different conditions (Fig. 1).

³⁴⁹ Unless otherwise noted, all statistical tests are two-sided, all error bars and error ribbons
³⁵⁰ denote bootstrap-estimated 95% confidence intervals across participants, and all reported *p*-values
³⁵¹ are corrected for multiple comparisons using the Benjamini-Hochberg procedure (Benjamini &
³⁵² Hochberg, 1995).

³⁵³ Functional neuroimaging data collected during story listening

³⁵⁴ We examined an fMRI dataset collected by Simony et al. (2016) that the authors have made publicly
³⁵⁵ available at arks.princeton.edu/ark:/88435/dsp015d86p269k. The dataset comprises neuroimaging
³⁵⁶ data collected as participants listened to an audio recording of a story (intact condition; 36 par-
³⁵⁷ ticipants), listened to temporally scrambled recordings of the same story (17 participants in the
³⁵⁸ paragraph-scrambled condition listened to the paragraphs in a randomized order and 36 in the
³⁵⁹ word-scrambled condition listened to the words in a randomized order), or lay resting with their
³⁶⁰ eyes open in the scanner (rest condition; 36 participants). Full neuroimaging details may be found
³⁶¹ in the original paper for which the data were collected (Simony et al., 2016). Procedures were
³⁶² approved by the Princeton University Committee on Activities Involving Human Subjects, and by
³⁶³ the Western Institutional Review Board (Puyallup, WA). All subjects were native English speakers
³⁶⁴ with normal hearing and provided written informed consent.

³⁶⁵ Hierarchical topographic factor analysis (HTFA)

³⁶⁶ Following our prior related work, we used HTFA (Manning et al., 2018) to derive a compact
³⁶⁷ representation of the neuroimaging data. In brief, this approach approximates the timeseries
³⁶⁸ of voxel activations (44,415 voxels) using a much smaller number of radial basis function (RBF)
³⁶⁹ nodes (in this case, 700 nodes, as determined by an optimization procedure; Manning et al., 2018).

370 This provides a convenient representation for examining full-brain activity patterns and network
371 dynamics. All of the analyses we carried out on the neuroimaging dataset were performed in
372 this lower-dimensional space. In other words, each participant's data matrix was a number-of-
373 timepoints (T) by 700 matrix of HTFA-derived factor weights (where the row and column labels
374 were matched across participants). Code for carrying out HTFA on fMRI data may be found as
375 part of the BrainIAK toolbox (Capota et al., 2017; Kumar et al., 2021), which may be downloaded
376 at brainiak.org.

377 **Principal components analysis (PCA)**

378 We applied group PCA (Smith et al., 2014) separately to the HTFA-derived representations of the
379 data (i.e., factor loadings) from each experimental condition. Specifically, for each condition, we
380 considered the set of all participants' T by 700 factor weight matrices. We used group PCA to project
381 these 700-dimensional matrices into a series of shared k -dimensional spaces, for $k \in \{3, 4, 5, \dots, 700\}$.
382 This yielded a set of number-of-participants matrices, each with T rows and k columns.

383 **Temporal decoding**

384 We sought to identify neural patterns that reflected participants' ongoing cognitive processing of
385 incoming stimulus information. As reviewed by Simony et al. (2016), one way of homing in on
386 these stimulus-driven neural patterns is to compare activity patterns across individuals. In partic-
387 ular, neural patterns will be similar across individuals to the extent that the neural patterns under
388 consideration are stimulus-driven, and to the extent that the corresponding cognitive representa-
389 tions are reflected in similar spatial patterns across people (Simony & Chang, 2020). Following this
390 logic, we used an across-participant temporal decoding test developed by Manning et al. (2018) to
391 assess the degree to which different neural patterns reflected ongoing stimulus-driven cognitive
392 processing across people. The approach entails using a subset of the data to train a classifier to
393 decode stimulus timepoints (i.e., moments in the story participants listened to) from neural pat-
394 terns. We use decoding (forward inference) accuracy on held-out data, from held-out participants,
395 as a proxy for the extent to which the inputted neural patterns reflected stimulus-driven cognitive
396 processing in a similar way across individuals.

397 **Forward inference and decoding accuracy**

398 We used an across-participant correlation-based classifier to decode which stimulus timepoint
399 matched each timepoint’s neural pattern. For a given value of k (i.e., number of principal compo-
400 nents), we first used group PCA to project the data from each condition into a shared k -dimensional
401 space. Next, we divided the participants into two groups: a template group, $\mathcal{G}_{\text{template}}$ (i.e., training
402 data), and a to-be-decoded group, $\mathcal{G}_{\text{decode}}$ (i.e., test data). We averaged the projected data within
403 each group to obtain a single T by k matrix for each group. Next, we correlated the rows of the two
404 averaged matrices to form a T by T decoding matrix, Λ . In this way, the rows of Λ reflected time-
405 points from the template group, while the columns reflected timepoints from the to-be-decoded
406 group. We used Λ to assign temporal labels to each timepoint (row) from the test group’s ma-
407 trix, using the row of the training group’s matrix with which it was most highly correlated. We
408 repeated this decoding procedure, but using $\mathcal{G}_{\text{decode}}$ as the template group and $\mathcal{G}_{\text{template}}$ as the
409 to-be-decoded group. Given the true timepoint labels (for each group), we defined the decoding
410 accuracy as the average proportion of correctly decoded timepoints, across both groups (where
411 chance performance is $\frac{1}{T}$). In Figures 2 and 3 we report the decoding accuracy for each condition
412 and value of k , averaged across $n = 100$ cross validation folds.

413 **Reverse inference**

414 To help interpret the brain activity patterns we found within the contexts of other studies, we
415 created summary maps of each principal component, for each experimental condition. Each
416 principal component comprises 700 “weights” on each of the HTFA-derived RBF nodes (see
417 *Hierarchical Topographic Factor Analysis*). For each node, we evaluated its RBF at the locations of
418 every voxel in the standard 2 mm MNI152 template brain and multiplied the RBF by the node’s
419 weight. The sum of these weighted RBF activation maps provides a full-brain image, in MNI152
420 space, of the given principal component (Fig. S3).

421 Next, we considered 80 topics estimated using Latent Dirichlet Allocation (Blei et al., 2003)
422 applied to 9,204 functional neuroimaging articles in the Neurosynth database (Rubin et al., 2017).
423 The topics, as well as associated brain maps identified using Neurosynth, were identified and
424 reported in several prior studies (Chen et al., 2020; Fox et al., 2014; Sul et al., 2017). The topic

425 labels for each topic were generated automatically with the following ChatGPT (OpenAI, 2023)
426 prompt: “Please help me come up with intuitive labels for topics I found by fitting a topic model
427 to thousands of neuroscience and psychology articles. I’ll paste in the top 10 highest-weighted
428 words for each topic, and I’d like you to respond with a suggested label. For each topic, please
429 respond with just the topic label and no other formatting or text. Here are the next topic’s top
430 words:” followed by a comma-separated list of the given topic’s top-weighted words reflected
431 in the Table S1. For some topics, ChatGPT responded with a longer-form response rather than a
432 concise topic label. In these instances, on a case-by-case basis, we used a second follow-up prompt
433 to achieve the given topic’s label: “Could you please come up with a more concise label for that
434 topic?”. We then manually identified a set of 11 cognitive labels that were intended to encapsulate
435 a representative range of widely studied low-level and high-level cognitive functions. In choosing
436 the set of cognitive labels, we jointly considered each topic’s ChatGPT-derived topic label, along
437 with the top-weighted words for the topic. We attempted to generate a concise set of labels that
438 still spanned the full set of cognitive functions reflected across the 80 topics. Topics that appeared
439 unrelated to specific cognitive functions (e.g., topics related to specific methods or clinical themes)
440 are designated with dashes in Table S1.

441 Finally, following an approach used in several prior studies (Chen et al., 2020; Fox et al., 2014;
442 Sul et al., 2017) we treated the correlation between a given component’s brain map and each topic’s
443 brain map as an approximate measure of how much the component was reflective of the given
444 topic. This resulted in a set of 80 “weights” (correlation coefficients) for each component’s brain
445 map, with one weight per Neurosynth-derived topic.

446 **Ranking cognitive processes**

447 We manually identified 11 cognitive labels spanning the set of 80 Neurosynth-derived topics:
448 cognitive control, language processing, memory, emotion, social cognition, spatial cognition, at-
449 tention, reward, sensory perception, motor control, and resting state. We then used ChatGPT
450 to automatically “rank” the processes from high-level to low-level using the following prompt:
451 “Please rank these cognitive processes from highest-level to lowest-level, where higher values
452 indicate higher-order or higher-level processes. Return the result as a csv file with a header row

453 and two columns: ‘Cognitive label’ and ‘Rank’. Here are the processes: cognitive control, lan-
454 guage processing, memory, emotion, social cognition, spatial cognition, attention, reward, sensory
455 perception, motor control, resting state”. Table S2 displays the output.

456 In the analysis presented in Figure 6E, we summarize difference in topic weightings across
457 experimental conditions. In particular, we sought to characterize how the dominant neural patterns
458 evoked by each experimental condition weighted on different cognitive functions. For each of the
459 top five principal components from each experimental condition (Fig. 5), we computed the average
460 weightings for each of the 11 manually identified (and ChatGPT-ranked) cognitive labels described
461 above (Tab. S2). We then fit a line separately for each experiment condition (x -values: cognitive
462 rank; y -values: weights). In carrying out this analysis, we used a bootstrap procedure to estimate
463 the variability in the slopes of the regression lines, whereby we repeated this process for each of
464 $n = 100$ iterations, each time resampling (with replacement) the set of observed ranks and weights.
465 This procedure yielded distributions of 100 estimated slopes for each experimental condition. We
466 used these distributions to compare the slopes across experimental conditions and to estimate 95%
467 confidence intervals.

468 Synthetic data

469 To help illustrate the relationship between informativeness and compressibility (Fig. 1), we gen-
470 erated four synthetic datasets, varying in informativeness and compressibility. Each dataset com-
471 prised simulated observations of $K = 25$ features across $N = 100$ timepoints, from each of $S = 10$
472 participants. To create each dataset, we first constructed a “template” matrix of N timepoints by K
473 features. We then generated participant-specific data by adding independent noise to each entry
474 in template matrix, drawn from the unit normal distribution (i.e., with a mean of 0 and a variance
475 of 1). We repeated this process for each participant, yielding S participant-specific matrices for
476 each dataset.

477 Since we estimate informativeness using the temporal decoding accuracy across participants,
478 highly informative data will tend to have observations that are highly timepoint specific. Relatively
479 uninformative data, in contrast, will tend to have more similar observations across timepoints. To
480 generate data with “high informativeness,” we constructed template matrices whose rows (ob-

481 servations) were drawn independently from zero-mean multivariate normal distributions. The
482 covariances of these distributions were determined according to the desired compressibility of
483 the data, as described below. We used a multi-step process to generate data with “low informa-
484 tiveness.” First we generated new template matrices using the same procedure as for the “high
485 informativeness” datasets. We then multiplied each matrix by a constant ($\rho = 0.1$) and computed
486 the cumulative sum of each matrix’s rows. This yielded matrices whose rows were highly similar
487 across observations.

488 Compressibility reflects the extent to which decoding accuracy is affected by reducing the num-
489 ber of components used to represent the data. Highly compressible data will tend to exhibit more
490 similarities across features, whereas less compressible data will tend to show greater independence
491 across features. To generate data with “high compressibility,” we set the covariance matrix of the
492 multivariate normal distribution to a toeplitz matrix whose first row was given by $[K, K - 1, \dots, 1]$.
493 To generate data with “low compressibility,” we set the covariance matrix to the identity matrix.

494 Template matrices for datasets with high informativeness and high compressibility, high in-
495 formativeness and low compressibility, low informativeness and high compressibility, and low
496 informativeness and low compressibility are displayed in Figure 1C. The corresponding decoding
497 curves are displayed in Figure 1D.

498 Data and code availability

499 All of the code used to produce the figures and results in this manuscript, along with links to the
500 corresponding data, may be found at github.com/ContextLab/pca_paper.

501 Acknowledgements

502 We acknowledge discussions with Rick Betzel, Luke Chang, Emily Finn, and Jim Haxby. Our
503 work was supported in part by NSF CAREER Award Number 2145172 to J.R.M. The content is
504 solely the responsibility of the authors and does not necessarily represent the official views of our
505 supporting organizations. The funders had no role in study design, data collection and analysis,
506 decision to publish, or preparation of the manuscript.

507 **Author contributions**

508 Conceptualization: J.R.M. and L.L.W.O. Methodology: J.R.M. and L.L.W.O. Implementation:
509 J.R.M. and L.L.W.O. Analysis: J.R.M. and L.L.W.O. Writing, Reviewing, and Editing: J.R.M. and
510 L.L.W.O. Funding acquisition: J.R.M. Supervision: J.R.M.

511 **References**

- 512 Adachi, Y., Osada, T., Sporns, O., Watanabe, T., Matsui, T., Miyamoto, K., & Miyashita, Y.
513 (2012). Functional connectivity between anatomically unconnected areas is shaped by collective
514 network-level effects in the macaque cortex. *Cerebral Cortex*, 22(7), 1586–1592.
- 515 Alvarez, S. A. (2002). *An exact analytical relation among recall, precision, and classification accuracy in
516 information retrieval* (Technical Report No. BCCS-02-01). Boston College.
- 517 Baldassano, C., Chen, J., Zadbood, A., Pillow, J. W., Hasson, U., & Norman, K. A. (2017). Discov-
518 ering event structure in continuous narrative perception and memory. *Neuron*, 95(3), 709–721.
- 519 Bassett, D. S., & Sporns, O. (2017). Network neuroscience. *Nature Neuroscience*, 20(3), 353–364.
- 520 Benjamini, Y., & Hochberg, Y. (1995). Controlling the False Discovery Rate: a practical and
521 powerful approach to multiple testing. *Journal of Royal Statistical Society, Series B*, 57, 289–300.
- 522 Blei, D. M., Ng, A. Y., & Jordan, M. I. (2003). Latent dirichlet allocation. *Journal of Machine Learning
523 Research*, 3, 993–1022.
- 524 Brovelli, A., Ding, M., Ledberg, A., Chen, Y., Nakamura, R., & Bressler, S. (2004). Beta oscillations in
525 a large-scale sensorimotor cortical network: directional influences revealed by Granger causality.
526 *Proceedings of the National Academy of Sciences, USA*, 101(26), 9849–9854.
- 527 Bullmore, E., & Sporns, O. (2009). Complex brain networks: graph theoretical analysis of structural
528 and functional systems. *Nature Reviews Neuroscience*, 10(3), 186–198.
- 529 Capota, M., Turek, J., Chen, P.-H., Zhu, X., Manning, J. R., Sundaram, N., ... Shin, Y. S. (2017).
530 *Brain imaging analysis kit*.

- 531 Chen, P.-H. A., Jolly, E., Cheong, J. H., & Chang, L. J. (2020). Intersubject representational
532 similarity analysis reveals individual variations in affective experience when watching erotic
533 movies. *NeuroImage*, 216(116851), doi.org/10.1016/j.neuroimage.2020.116851.
- 534 Cole, M. W., Bassett, D. S., Power, J. D., Braver, T. S., & Petersen, S. E. (2014). Intrinsic and
535 task-evoked network architectures of the human brain. *Neuron*, 83(1), 238–251.
- 536 Dhamala, M., Rangarajan, G., & Ding, M. (2008). Analyzing information flow in brain networks
537 with nonparametric Granger causality. *NeuroImage*, 41(2), 354–362.
- 538 Finn, E. S., Scheinost, D., Finn, D. M., Shen, X., Papademetris, X., & Constable, R. T. (2017).
539 Can brain state be manipulated to emphasize individual differences in functional connectivity.
540 *NeuroImage*, 160, 140–151.
- 541 Finn, E. S., Shen, X., Scheinost, D., Rosenberg, M. D., Huang, J., Chun, M. M., ... Constable, R. T.
542 (2015). Functional connectome fingerprinting: identifying individuals using patterns of brain
543 connectivity. *Nature Neuroscience*, 18, 1664–1671.
- 544 Fox, A. S., Chang, L. J., Gorgolewski, K. J., & Yarkoni, T. (2014). Bridging psychology and
545 genetics using large-scale spatial analysis of neuroimaging and neurogenetic data. *bioRxiv*,
546 doi.org/10.1101/012310.
- 547 Glerean, E., Salmi, J., Lahnakoski, J. M., Jääskeläinen, I. P., & Sams, M. (2012). Functional magnetic
548 resonance imaging phase synchronization as a measure of dynamic functional connectivity.
549 *Brain Connectivity*, 2(2), 91–101.
- 550 Gratton, C., Laumann, T. O., Nielsen, A. N., Greene, D. J., Gordon, E. M., Gilmore, A. W., ...
551 Petersen, S. E. (2018). Functional brain networks are dominated by stable group and individual
552 factors, not cognitive or daily variation. *Neuron*, 98(2), 439–452.
- 553 Hasson, U., Yang, E., Vallines, I., Heeger, D. J., & Rubin, N. (2008). A hierarchy of temporal
554 receptive windows in human cortex. *The Journal of Neuroscience*, 28(10), 2539–2550.
- 555 Korzeniewska, A., Crainiceanu, C. M., Kus, R., Franaszczuk, P. J., & Crone, N. E. (2008). Dynamics
556 of event-related causality in brain electrical activity. *Human Brain Mapping*, 29(10).

- 557 Kumar, M., Anderson, M. J., Antony, J. W., Baldassano, C., Brooks, P. P., Cai, M. B., ... Norman,
558 K. A. (2021). BrainIAK: the brain image analysis kit. *Aperture*, *In press*.
- 559 Lerner, Y., Honey, C. J., Silbert, L. J., & Hasson, U. (2011). Topographic mapping of a hierarchy of
560 temporal receptive windows using a narrated story. *The Journal of Neuroscience*, 31(8), 2906–2915.
- 561 Lynn, C. W., & Bassett, D. S. (2021). Quantifying the compressibility of complex networks.
562 *Proceedings of the National Academy of Sciences, USA*, 118(32), e2023473118.
- 563 Mack, M. L., Preston, A. R., & Love, B. C. (2020). Ventromedial prefrontal cortex compression during concept learning. *Nature Communications*, 11(46), doi.org/10.1038/s41467-019-13930-8.
- 565 Manning, J. R. (2020). Context reinstatement. In M. J. Kahana & A. D. Wagner (Eds.), *Handbook of
566 human memory*. Oxford University Press.
- 567 Manning, J. R., Zhu, X., Willke, T. L., Ranganath, R., Stachenfeld, K., Hasson, U., ... Norman,
568 K. A. (2018). A probabilistic approach to discovering dynamic full-brain functional connectivity
569 patterns. *NeuroImage*, 180, 243–252.
- 570 Norman, K. A., Polyn, S. M., Detre, G. J., & Haxby, J. V. (2006). Beyond mind-reading: multi-voxel
571 pattern analysis of fMRI data. *Trends in Cognitive Sciences*, 10(9), 424–430.
- 572 OpenAI. (2023, March). *ChatGPT*. Personal communication.
- 573 Owen, L. L. W., Chang, T. H., & Manning, J. R. (2021). High-level cognition during story listening is
574 reflected in high-order dynamic correlations in neural activity patterns. *Nature Communications*,
575 12(5728), doi.org/10.1038/s41467-021-25876-x.
- 576 Owen, L. L. W., Muntianu, T. A., Heusser, A. C., Daly, P., Scangos, K. W., & Manning, J. R. (2020). A
577 Gaussian process model of human electrocorticographic data. *Cerebral Cortex*, 30(10), 5333–5345.
- 578 Preti, M. G., Bolton, T. A. W., & Van De Ville, D. (2017). The dynamic functional connectome:
579 state-of-the-art and perspectives. *NeuroImage*, 160, 41–54.
- 580 Regev, M., Simony, E., Lee, K., Tan, K. M., Chen, J., & Hasson, U. (2018). Propagation of information
581 along the cortical hierarchy as a function of attention while reading and listening to stories.
582 *Cerebral Cortex*.

- 583 Rogers, B. P., Morgan, V. L., Newton, A. T., & Gore, J. C. (2007). Assessing functional connectivity
584 in the human brain by fMRI. *Magnetic Resonance Imaging*, 25(11), 1347–1357.
- 585 Rubin, T. N., Kyojo, O., Gorgolewski, K. J., Jones, M. N., Poldrack, R. A., & Yarkoni, T. (2017).
586 Decoding brain activity using a large-scale probabilistic functional-anatomical atlas of human
587 cognition. *PLoS Computational Biology*, 13(10), e1005649.
- 588 Rubinov, M., & Sporns, O. (2010). Complex network measures of brain connectivity: uses and
589 interpretations. *NeuroImage*, 52, 1059–1069.
- 590 Scangos, K. W., Khambhati, A. N., Daly, P. M., Owen, L. L. W., Manning, J. R., Ambrose, J. B.,
591 ... Chang, E. F. (2021). Biomarkers of depression symptoms defined by direct intracranial
592 neurophysiology. *Frontiers in Human Neuroscience*, In press.
- 593 Shannon, C. E. (1948). A mathematical theory of communication. *Bell System Technical Journal*,
594 27(3), 379–423.
- 595 Simony, E., & Chang, C. (2020). Analysis of stimulus-induced brain dynamics during naturalistic
596 paradigms. *NeuroImage*, 216, 116461.
- 597 Simony, E., Honey, C. J., Chen, J., & Hasson, U. (2016). Dynamic reconfiguration of the default
598 mode network during narrative comprehension. *Nature Communications*, 7(12141), 1–13.
- 599 Sizemore, A. E., Giusti, C., Kahn, A., Vettel, J. M., Betzel, R. F., & Bassett, D. S. (2018). Cliques and
600 cavities in the human connectome. *Journal of Computational Neuroscience*, 44(1), 115–145.
- 601 Smith, S. M., Beckmann, C. F., Andersson, J., Auerbach, E. J., Bijsterbosch, J., Douaud, G., ...
602 Glasser, M. F. (2013). Resting-state fMRI in the Human Connectome Project. *NeuroImage*, 80,
603 144–168.
- 604 Smith, S. M., Fox, P. T., Miller, K. L., Glahn, D. C., Fox, P. M., Mackay, C. E., ... Beckmann,
605 C. F. (2009). Correspondence of the brain's functional architecture during activation and rest.
606 *Proceedings of the National Academy of Sciences, USA*, 106(31), 13040–13045.
- 607 Smith, S. M., Hyvärinen, A., Varoquaux, G., Miller, K. L., & Beckmann, C. F. (2014). Group-PCA
608 for very large fMRI datasets. *NeuroImage*, 101, 738–749.

- 609 Smith, S. M., Vidaurre, D., Beckmann, C. F., Glasser, M. F., Jenkinson, M., Miller, K. L., ... Van
610 Essen, D. C. (2013). Functional connectomics from resting-state fMRI. *Trends in Cognitive Sciences*,
611 17(12), 666–682.
- 612 Sporns, O., & Betzel, R. F. (2016). Modular brain networks. *Annual Review of Psychology*, 67,
613 613–640.
- 614 Sporns, O., & Honey, C. J. (2006). Small worlds inside big brains. *Proceedings of the National Academy
of Sciences, USA*, 103(51), 19219–19220.
- 616 Sporns, O., & Zwi, J. D. (2004). The small world of the cerebral cortex. *Neuroinformatics*, 2(2),
617 145–162.
- 618 Srinivasan, R., Winter, W. R., Ding, J., & Nunez, P. L. (2007). EEG and MEG coherence: Measures of
619 functional connectivity at distinct spatial scales of neocortical dynamics. *Journal of Neuroscience
Methods*, 166, 41–52.
- 621 Sul, S., Güroğlu, B., Crone, E. A., & Chang, L. J. (2017). Medial prefrontal cortical thinning
622 mediates shifts in other-regarding preferences during adolescence. *Scientific Reports*, 7(8510),
623 doi.org/10.1038/s41598-017-08692-6.
- 624 Tomasi, D., & Volkow, N. D. (2011). Association between functional connectivity hubs and brain
625 networks. *Cerebral Cortex*, 21, 2003–2013.
- 626 Yeo, B. T. T., Krienen, F. M., Sepulcre, J., Sabuncu, M. R., Lashkari, D., Hollinshead, M., ... Buckner,
627 R. L. (2011). The organization of the human cerebral cortex estimated by intrinsic functional
628 connectivity. *Journal of Neurophysiology*, 106(3), 1125–1165.